scientific reports

Check for updates

OPEN

Experimental study on the influence of turbulence on hail impacts

Yimin Dai[1,2]✉, Wei Wang[1,2], Ying Xu[1,2], Yixin Li[1,2] & Taiting Liu[1,2]

Hailstorms, characterized by their intensity, are often accompanied by strong winds and heavy rain, posing significant destructive potential. Data indicate that the economic losses caused by hail to buildings, particularly solar panels, have been increasing annually. However, research on the hail resistance of photovoltaic panels has predominantly focused on the isolated effects of hail impacts and wind loads, neglecting the coupling effects between wind and hail. In this study, a device was designed to couple both wind and hail. The effects of turbulence, hail size, and velocity on hail impact behavior were systematically studied and quantified. A predictive formula for the peak load of hail impact on structures was established. The results indicate that the impact of turbulence on hail is significant. When turbulence intensity varies with hail velocity, hail impact force increases as turbulence decreases and hail velocity increases. When both turbulence and hail diameter vary, the impact force of smaller hailstones shows less variation with increasing turbulence. According to variance analysis, hail velocity is the most significant factor affecting hail impact, followed by hail diameter and finally turbulence. The regression equation is given by $F = -0.624I_u + 5116.25D + 7.85V_{hail} - 259.709$, where F represents the peak impact force in Newtons (N), I_u denotes the turbulence intensity, D is the hail diameter in meters (m), and V_{hail} is the hail velocity in meters per second (m/s).

Keywords Wind-hail coupling, Wind tunnel test, Impact test, Turbulence, Multivariate linear regression

Hailstorms are highly destructive, often accompanied by strong winds and heavy rain, resulting in significant damage. Data indicate that economic losses caused by hail damage to buildings, particularly solar panels, have been increasing annually[1,2]. With the continuous advancement of photovoltaic technology, the advantages of its energy conversion efficiency, economic benefits, and environmental value are becoming increasingly evident. Photovoltaic power generation is expected to proliferate rapidly over the next few decades[3], potentially becoming one of the most crucial energy sources in the future. The development of the photovoltaic industry also imposes higher demands on its disaster resilience. In regions with abundant wind resources, wind and hail disasters are common occurrences[4]. Therefore, studying the mechanisms of wind and hail resistance in photovoltaic structures is of great significance.

McDonald et al.[5] combined experimental methods and field measurements to detect and evaluate the impact characteristics of hail particles of different diameters. Ding et al.[6] conducted numerical simulations to study the hail resistance of greenhouse glass under impacts from hailstones of various sizes. The results indicated that the impact of multiple hailstones on a glass pane is not equivalent to the impact of a single hailstone. A 4 mm thick glass pane can meet the hail resistance requirements of most glass greenhouses. It is recommended that the length-to-width ratio of the glass panes be approximately 1.5. Kilikevičienė et al.[7–9] designed and constructed a hail simulation platform to study the effects of hail particle impacts under different parameters on the crystal structure of photovoltaic modules and their power generation capacity. Based on their findings, they proposed optimization design solutions for photovoltaic panels. Hassan[10] conducted a CFD simulation to model the wind pressure on solar photovoltaic panels under varying turbulence intensities. The study revealed that photovoltaic panels experience significant lift and drag forces when subjected to wind loads, necessitating the quantification of an adequate safety factor to prevent damage. Stathopoulos et al.[11] experimentally investigated the wind pressure distribution characteristics of photovoltaic panels attached to flat roofs. The study found that the net pressure coefficients for different configurations were influenced by the panel tilt angle at a critical wind direction of 135°, with the rear panels experiencing greater wind suction than the front panels. The height of the building had little

[1]Hunan Provincial Key Laboratory of Structural Wind and Vibration Control, Xiangtan 411201, China. [2]School of Civil Engineering, Hunan University of Science and Technology, Xiangtan 411201, China. ✉email: 617275190@qq.com

effect on the overall load on the solar collectors, while panels at critical azimuth angles experienced higher net loads. Chung et al.[12] experimentally determined the wind loads on freestanding solar panel arrays. When the wind incidence angle ranged from 0° to 60°, the lift coefficient varied in a U-shaped pattern with the tilt angle. The formation of strong upwind corner vortices caused the right half of the inclined panels to experience greater lift when the wind incidence angle was between 30° and 45°. Chen Wei et al.[13] studied the effects of roof type, height, and photovoltaic array layout on the net wind loads of photovoltaic panels. Zou[14] and Yin[15] conducted wind tunnel tests to obtain the surface wind pressure distribution of tracking photovoltaic structures. The results showed that the wind direction angle and tilt angle significantly affected the wind loads on the photovoltaic panels. Ma et al.[16] analyzed the impact of interference effects within an array on the wind load values of photovoltaic panels based on different wind direction angles, tilt angles, and the number of photovoltaic panels. The results indicated that when the photovoltaic panels face the wind or are back to the wind, the upstream panels significantly shield the downstream panels, with the shielding effect positively correlated with the tilt angle. The wind load on the downstream panels tends to stabilize starting from the fourth row. Lou et al.[17] studied the shape coefficients and group shielding effects of ultra-large array photovoltaic panels using a combination of wind tunnel tests and CFD numerical simulations. The results showed that the shielding effect at a tilt angle of 20° was significantly greater than that at a tilt angle of 12°, and the shielding effect increased with the number of upstream photovoltaic panels.

Research on the wind and hail resistance of structures often isolates the impact effects of hail from wind loads, neglecting the coupling effects between wind and hail. Studies have shown that wind is an indispensable factor when assessing the losses caused by wind and hail hazards[18–21]. Based on this, this paper employs wind tunnel experiments and innovatively designs a wind-hail coupling test system to comparatively study the impact behavior patterns of hail under different turbulence conditions, hail sizes, and velocities. This research provides a reference for the study of disaster mitigation and prevention of structural wind and hail damage.

Experimental procedure

Wind-hail coupling test platform

This test study was carried out at the Wind Engineering Test and Research Centre of Hunan University of Science and Technology, which houses a flat DC inhalation type single test section low-speed wind tunnel. The test section of the wind tunnel measures 4.0 m in width, 3.0 m in height, and 21.0 m in length, with an adjustable wind speed range of 0–30 m/s.

To simulate wind-hail coupling situations, a hailstorm simulation launch system and an acquisition system suitable for wind tunnel tests were developed independently.

This test incorporates a self-designed and manufactured air gun device as a hail simulation launching system. The device consists of a manual valve, air pressure gauge, external air pump, firing tube, and adjustable standoffs. Regulating the air pressure can control the speed of the hail launch, tuning the adjustment stand can change the angle of the hail launch, and replacing different launch tube diameters can achieve multiple diameters of the launch tube. (Fig. 1).

In this case, the hail-forming mold consists of two polypropylene hemisphere molds with a small hole in the upper half, mainly for removing excess water and preventing stress concentration. The molds are shown in Fig. 2. From Fig. 2, it is evident that the mold can produce hail particles that meet the test requirements.

In Fig. 1: where: 1- solar array, 2-force measurement and acquisition system,3-velocity monitoring system, 4-fill light, 5-velocity monitoring backdrop, 6-loading device, 7-launcher bracket, 8-launcher, 9- Turbulent Flow Instrumentation (TFI), A-wind condition simulation section, B-wind-hail simulation section.

A hail velocity measurement device, a wind velocity measurement device, and a panel impact measurement device make up the acquisition system. In this paper, a high-speed camera recorded the hail launch velocity and monitored the hail fragmentation state, with a frames rate of 1000 frames per second. Throughout the entire experiment, flicker-free supplementary lighting was used to ensure adequate illumination for the imaging process. Wind speed and turbulence at a height of 30 cm (at the same height as the solar panel model) upstream of the building were collected by turbulent flow instrumentation (TFI), with a test sampling frequency of 333 Hz. The sampling time was approximately 30 s, a total of 10 000 samples were taken. The force measuring instrument used was the DYX-306 pressure sensor, with a sensitivity of less than 2.0 ± 0.05mV/V, non-linearity of less than $\pm 0.03\%$ F-S and a range of 0-2000N. This sensor measures only the normal impact force of hail. Studies have shown that when sliding at high speeds (up to 10 m/s), the friction between ice and target is almost zero (coefficient of kinetic friction less than 0.01)[22], as a film of water is generated between the ice and the target during the sliding process. The normal component of the impact velocity is the main factor causing damage to the solar panel, as there is hardly any friction during the impact, only pressure exists on the panel[23]. Therefore, only the normal impact force of the hail is investigated in this test. The output signal collector used is D.R300A handheld force measuring instrument. This system can accurately record the output signal time course according to the sampling frequency set by the instrument. It can also perform preliminary pre-processing with a non-linearity better than 0.01% and an accuracy better than 0.1%; the maximum sampling frequency is 12800 Hz.

The target model for this test was a solar panel 290 mm in length, 240 mm in width, 30 mm in thickness, and weighing 1 kg. The solar panel structure from top to bottom consisted of glass, EVA, CELLs, EVA, back sheet, and a thickened bezel. This solar panel is representative of solar arrays installed on most bridges. The model was mounted with pallet brackets (Fig. 3) at a height of 30cm above the ground.

To ensure the applicability and accuracy of this force measurement system in measuring hail impact forces under wind and hail flow fields, hail impact forces under windless conditions were first measured based on the experimental system. Figure 4 shows the force measurement results of 3.2cm diameter hail impacting a solar panel at a speed of 22.43m/s and an angle of attack of 45° under this experimental system. Comparing this

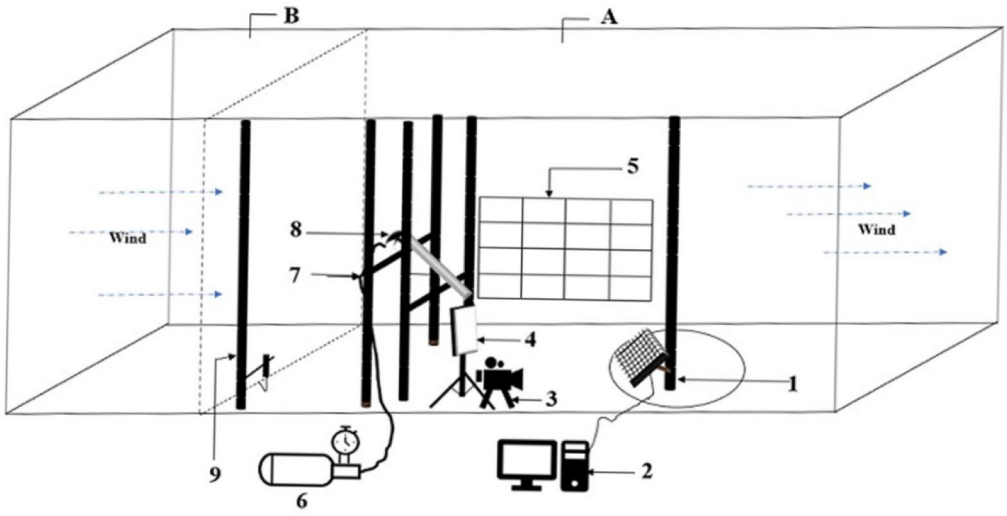

(a)

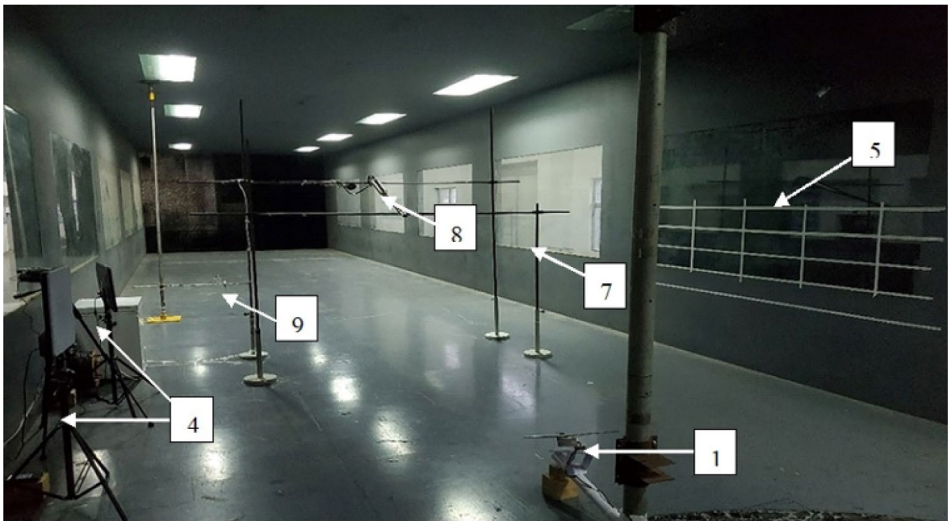

(b)

Figure 1. Wind-hail coupling test platform.

Figure 2. Hail mold and forming hail drawing.

Figure 3. Model of the solar panel.

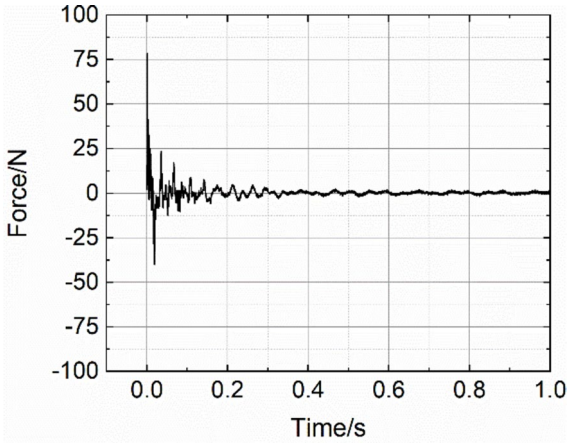

Figure 4. Experimental impact load–time histories of hail in this system.

result with the test results of KiliKevičienė[14] where a 4 cm hailstone impacted the PV panel vertically at a speed of 22.61 m/s, the results showed that the system is capable of measuring the peak force and general force pulse shape reasonably well. In summary, this force measurement system can be used for impact force measurements of hail in wind and hail flow fields.

Test load

The data shows that the size of hail particles in hailstorms is mainly between 0.5 and 3 cm [24], nd the test hail diameters were 2.8 cm and 3.2 cm, consistent with the realistic range specified in GB/T 27,957–2011 Hail Grades. The artificial simulated hail parameters in this experiment are shown in Table. 1.

The experiment simulated the empty wind field (E) and three turbulence conditions A, B, and C using the combined baffle grille method (Fig. 5). The Composite Baffle Grating Method is a technique utilized in fluid mechanics experiments, particularly in wind tunnel testing or other fluid dynamics evaluations. This method involves the use of multiple baffles and grating structures to alter and control fluid flow characteristics, such as turbulence intensity and velocity distribution. The Composite Baffle Grating Method effectively simulates various flow conditions, thereby allowing for more precise measurement and analysis of fluid behavior and its impact on test objects. Average wind speed profiles and turbulence profiles of each simulated wind condition are shown in Fig. 6. The solid line represents wind speed, while the dashed line represents turbulence intensity.

Diameter (mm)	Density (g/mm^3)	Mass (g)
28	0.9	10.33
32	0.9	15.43

Table 1. Related parameters of hail with different particle sizes.

(a) (b) (c)

Figure 5. Simulation of turbulent fields.

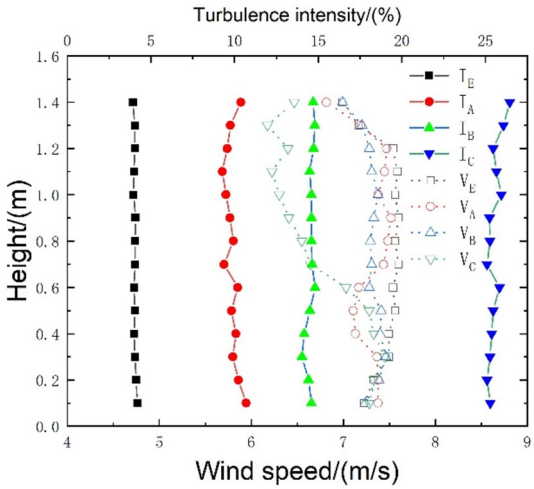

Figure 6. Average wind speed profiles and turbulence profiles of simulated wind conditions.

The test took place in the wind-hail coupling platform, with turbulence intensity, hail size, and velocity as the various factors. Four levels of turbulence intensity variation, two levels of particle size variation, and five levels of velocity variation were used for the combined experiments, resulting in a total of 40 test conditions. The specific working conditions are shown in Table. 2.

Hail diameter (cm)	Hail velocity (m/s)	Turbulence intensity (%)
2.8	18.7	2.5/8.5/13.5/25.5
2.8	20.7	2.5/8.5/13.5/25.5
2.8	22.5	2.5/8.5/13.5/25.5
2.8	24.5	2.5/8.5/13.5/25.5
2.8	27.8	2.5/8.5/13.5/25.5
3.2	18.7	2.5/8.5/13.5/25.5
3.2	20.7	2.5/8.5/13.5/25.5
3.2	22.5	2.5/8.5/13.5/25.5
3.2	24.5	2.5/8.5/13.5/25.5
3.2	27.8	2.5/8.5/13.5/25.5

Table 2. Table of test conditions.

Results and discussion

Effect of turbulence intensity on hail impact behavior

The experiment investigated the impact behavior law of a 2.8 cm diameter hail particle impacting a solar array with a velocity of 24.5 m/s and an attack angle of 45°, using turbulence intensity as a variable. To analyze the impact behavior, Fig. 7 illustrates the initial moment of impact of a single hailstone under varying turbulence intensities.

Figure 7 shows that as turbulence intensity increases, the hail impact duration becomes longer, the time to reach the peak impact force is delayed, and the peak impact force decreases. The peak impact load of hailstones is the smallest at 25.5% turbulence, which is about 21.84% lower than that at 2.5% turbulence. Additionally, as turbulence intensity increases, the shape of the hail impact time curve becomes more irregular. The author believes this may be due to the presence of numerous small vortices in the flow field. The larger the turbulence intensity, the more severe the destruction of laminar flow, and there is not only slipping but mixing between adjacent laminar flow layers. This irregular fluid motion influences hailstone impact behavior.

Figures 8 and 9 show the impact curves and surface plots of hail under different impact conditions. Figure 8a shows the comparison curves of the variation in hail impact force with turbulence intensity for different hail diameters at a hail velocity of 24.5 m/s. Figure 8a indicates a negative correlation between hailstone impact force and the degree of turbulence intensity, with the impact force decreasing as turbulence intensity increases. Additionally, the larger the hailstone diameter, the greater the decrease in peak impact force. The large interval between the two curves suggests that hail size significantly affects the hail impact force, with larger sizes resulting in higher impact forces. Figure 8b shows the response surface of the impact force under the joint influence of hail size and turbulence intensity when the hailstone velocity is 24.5 m/s. Figure 8b demonstrates that the impact force of the hail increases with increasing hail size and decreasing turbulence intensity. The maximum impact force occurs when the hailstone diameter is 3.2 cm and the turbulence is 2.5%, with a value of 102.6 N. The minimum impact force occurs when the hailstone diameter is 2.8 cm and the turbulence is 25.5%, with a value of 60 N. When turbulence intensity ranges from 13.5 to 25.5% and the hailstone diameter ranges from 3.0

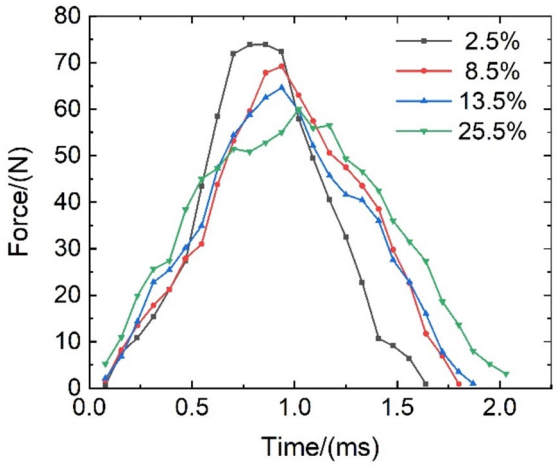

Figure 7. Experimental impact load–time histories of hail.

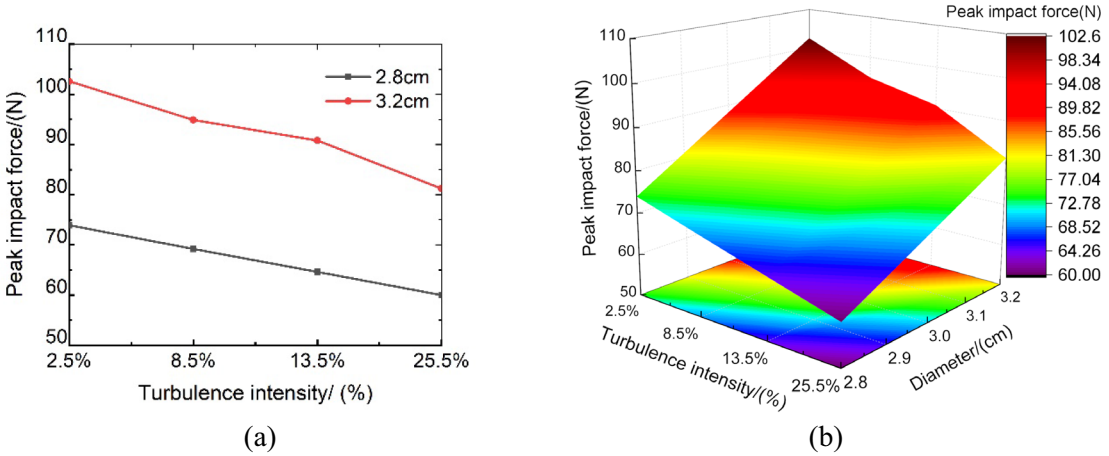

Figure 8. Impact force variation patterns at different turbulence intensities and hail diameters.

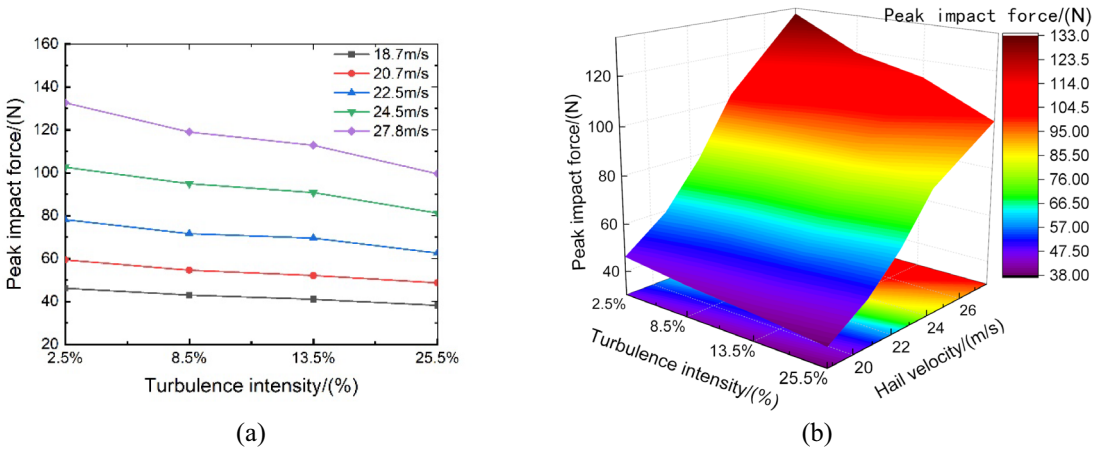

Figure 9. Impact force variation patterns at different turbulence intensities and hail velocity.

cm to 3.2 cm, the response surface is steeper, indicating a greater slope, which means that the hailstone impact force varies more in this area. As the hailstone size increases, the effect of turbulence intensity on the impact force becomes more pronounced.

Figure 9a shows a graph comparing the variation of hail with turbulence intensity at different velocities for a hail particle size of 3.2cm. From Fig. 9a, it can be seen that the hail impact force decreases with the increase of turbulence intensity and the decrease of hail velocity. Figure 9b shows the response surface of falling stone impact force under the influence of the joint change of hail velocity and turbulence intensity when the hail diameter is 3.2 cm. From Fig. 9b, it can be seen that the maximum impact force occurs when the hail velocity is 27.78 m/s and turbulence is 2.5%, while its value is 132.6 N. The minimum impact force occurs when the hail velocity is 18.7 m/s and the turbulence is 25.5%, while its value is 38.2N. When the turbulence is 13.5%-25.5% and the hail velocity is 26–-28m/s, this section of the graph is smoother, indicating that higher turbulence intensity has a greater impact on the impact force of hail particles at higher speeds.

The 3D surface plot of hail impact loads is shown in Fig. 10. Figure 10 provides a clearer and visual representation of the effect of each factor on hail impact. From Fig. 10, it can be seen that the hail size, hail velocity, and turbulence intensity have distinct effects on the hailstone impact force. As the size increases, the velocity increases, turbulence intensity decreases, and the impact of the hailstone increases.

Analysis of variance (ANOVA)

Univariate multi-factor ANOVA is a regression analysis and ANOVA performed on whether an independent variable is influenced by one or more variables. Using this ANOVA process, it is possible to test the question of whether there are differences in the means between different groups due to the influence of different factors in order to analyze the role of each factor.

The sum of the squares, variance, P-values, and F-values for each parameter is obtained by ANOVA to quantify the effect of each parameter on hail impact, as shown in Table. 3.

Table 3 shows that the effect of factors on hail impact can be assessed based on F-statistics. The order of influence of each factor on hail impact is: hail velocity > hail diameter > turbulence intensity. The P-values of all

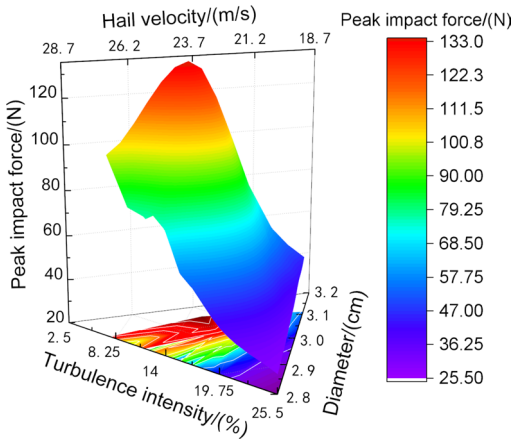

Figure 10. 3D surface view of hail impact.

Factors	S_T	d	mean square		F	Sig
Turbulence intensity	1147.70	3	382.569	19.706		< 0.0001
Diameter	4188.16	1	4188.162	215.733		< 0.0001
Velocity	23,668.2	4	5917.064	304.789		< 0.0001
$R^2 = 0.980 (Ra^2 = 0.974)$						

Table 3. Variance analysis of factors on hail impact.

factors are less than 0.05, indicating statistically significant correlations between hail impact forces and individual parameters. These conclusions are consistent with the above analysis.

Multiple linear regression

From Fig. 11, the histogram of standardized residuals is in the shape of an inverted bell and is more symmetrical on both the left and right sides. Figure 12 shows that the standardized residual P-P plot has scattered points close to the diagonal line, indicating that the residuals are normally distributed. Figure 13 shows that, with the vertical axis at 0 as the symmetry axis, the scattered points are evenly distributed randomly on both sides, and the variance is homogeneous. Table 4 shows that dw = 1.824; according to the Durbin-Watson table, the residuals are independent. The VIF values are all below 4, indicating that there is no significant multicollinearity among the variables. Thus, it is possible to perform multiple linear regression fits.

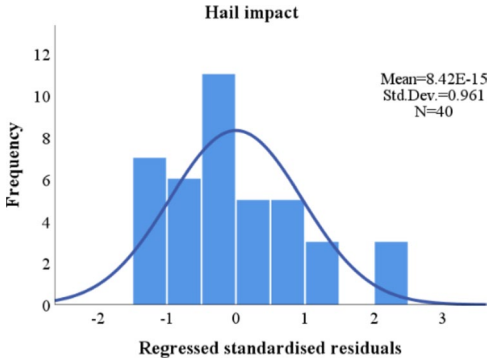

Figure 11. Regression standardized residual plot.

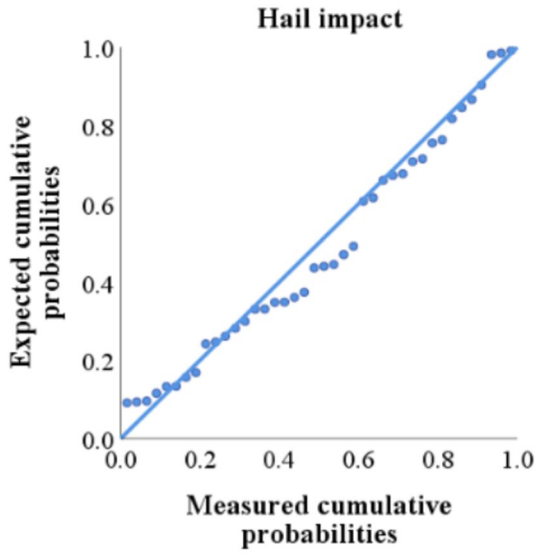

Figure 12. Standard P-P plot of regression-standardized residuals.

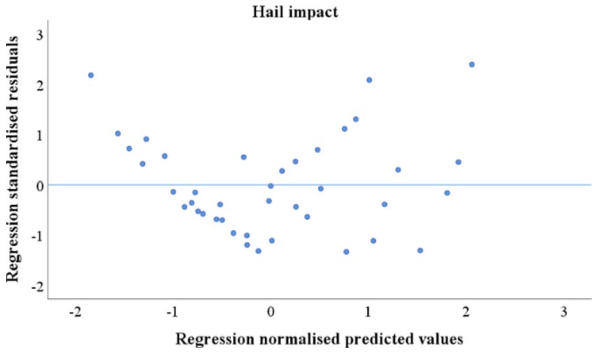

Figure 13. Residual scatter plot.

	Quadratic sum	d	Mean square	F	Sig
Regression	28,681.182	3	9560.394	372.174	< 0.0001
Residual	924.766	36	25.688		
Sum	29,605.948	39			
R^2	0.969	Ra^2	0.966	Dw	1.824

Table 4. Variance analysis of factors on hail impact.

In order to solve and predict the impact force of hail on structures through numerical calculation methods, which can provide references for engineering design, multiple regression analysis is utilized with experimental data. The regression model is assumed to be as follows:

$$F = aI_{\mathrm{u}} + bD + cV_{hail} + d \tag{1}$$

where F is the peak hail impact structure load, N, I_{u} is the turbulence intensity, D is the hail diameter, m, and V_{hail} is the hail velocity, m/s.

The test data are fitted by fitting the model, and the fitted equation is:

$$F = -0.624I_{\mathrm{u}} + 5116.25D + 7.85V_{hail} - 259.709 \tag{2}$$

Table. 4 shows that the R-squared is 0.984, the F-value is 372.174, and t significance level is less than 0.001, which means that the regression equation fits well. The sketches in Table. 5 indicate that hail velocity, size, and turbulence intensity are all significant to hail impact. The standardized partial regression coefficients show that hail velocity is the most influential factor in the impact, followed by hail size, with turbulence intensity having the least impact.

Conclusions

In this paper, a wind and hail coupling test platform applicable to wind tunnel tests was innovatively designed. The influence of turbulence intensity, hail size and velocity on hail impact behavior was systematically studied on this platform. The findings in the current study are as follows: The effect of turbulence intensity on hail impact is significant. As turbulence intensity increases, the hail impact duration becomes longer, the time to reach the peak impact force slows down, and the peak impact force decreases. A multiple linear regression analysis was used to derive a model for the peak hail impact force on photovoltaic panels, resulting in a well-fitted model. The regression equation is given by $F = -0.624I_{\mathrm{u}} + 5116.25D + 7.85V_{hail} - 259.709$, where F represents the peak impact force in Newtons (N), I_{u} denotes the turbulence intensity, D is the hail diameter in meters (m), and

	Standardized coefficient			Covariance statistics	
	Beta	t	Sig	Tolerance	VIF
		-19.270	< 0.0001		
Turbulence Intensity	-0.194	-6.583	< 0.0001	1.000	1.000
Diameter	0.376	12.769	< 0.0001	1.000	1.000
Velocity	0.889	30.169	< 0.0001	1.000	1.000

Table 5. Variance analysis of factors on hail impact.

V_{hail} is the hail velocity in meters per second (m/s). The influence degree is in order: hail velocity > hail diameter > turbulence intensity based on Analysis of Variance.

Data availability

Data is available upon request; researchers interested in reviewing our data should contact Yimin DAI at 617275190@qq.com.

Received: 24 April 2024; Accepted: 1 August 2024
Published online: 07 August 2024

References

1. Lin, Y. *et al.* Urbanization-induced land and aerosol impacts on storm propagation and hail characteristics. *J. Atmos. Sci.* **78**(3), 925–947 (2021).
2. Tang, B. H., Gensini, V. A. & Homeyer, C. R. Trends in United States large hail environments and observations. *NPJ Clim. Atmos. Sci.* **2**(1), 1–7 (2019).
3. Liu, C. J., Deng, X. W. & Liu, J. Dynamic response of saddle membrane structure under hail impact. *Eng. Struct.* **214**, 110597 (2020).
4. Macdonald, J. R. & Stack, M. M. Some thoughts on modelling hail impact on surfaces. *J. Bio-and Tribo-Corrosion* **7**(2), 1–7 (2021).
5. Macdonald, D. J. R. & Stack, M. M. Some thoughts on modelling hail impact on surfaces. *J. Bio Tribo-Corros.* **7**(2), 1–7 (2021).
6. Ding, M. *et al.* Numerical simulation on damage behavior of greenhouse glass under hail impact. *Trans. CSAE* **28**(01), 202–207 (2012).
7. KiliKevičienė, K. *et al.* Tests of hail simulation and research of the resulting impact on the structural reliability of solar cells. *Eksploatacja i Niezawodność* **21**(2), 96 (2019).
8. Kilikevičienė, K. *et al.* Research of the energy losses of photovoltaic (PV) modules after hail simulation using a newly-created testbed. *Energies* **12**(23), 4537 (2019).
9. Makarskas, V. *et al.* Investigation of the influence of hail mechanical impact parameters on photovoltaic modules. *Eng. Fail. Anal.* **124**, 105309 (2021).
10. Irtaza, H. & Agarwal, A. CFD simulation of turbulent wind effect on an array of ground-mounted solar PV panels[J/OL]. *J. Inst. Eng. Ser. A* **99**(2), 205–218 (2018).
11. Stathopoulos, T., Zisis, I. & Xypnitou, E. Local and overall wind pressure and force coefficients for solar panels. *J. Wind Eng. Ind. Aerodyn.* **125**, 195–206 (2014).
12. Chung, P. H. *et al.* Wind loads on a PV array. *Appl. Sci.* **9**(12), 2466 (2019).
13. Chen, W. & Zhu, Z. Numerical simulation of wind turbulence by DSRFG and identification of the aerodynamic admittance of bridge decks. *Eng. Appl. Comput. Fluid Mech.* **14**(1), 1515–1535 (2020).
14. Yunfeng, Z. *et al.* Comparison of wind load standard values of tracking photovoltaic (PV) structure with wind tunnel test values. *J. Central South Univ. (Natural Science Edition)* **53**(04), 1331–1340 (2022).
15. Meizi, Y. *et al.* Wind tunnel test study on wind load of single-row tracking photovoltaic structure. *Trans. Railway Sci. Eng.* **17**(09), 2354–2362 (2020).
16. Wenyong, Ma. *et al.* Wind tunnel test study on wind load interference effect of photovoltaic array. *Exp. Fluid Mech.* **35**(04), 19–25 (2021).
17. Wenjuan, L. *et al.* Study of shielding effect on shape coefficient of super-large photovoltaic arrays. *J. Build. Struct.* **42**(05), 47–54 (2021).
18. Changnon, S. A. Jr. Hailstreaks. *J. Atmos. Sci.* **27**(1), 109–125 (1970).
19. Schuster, S. S., Blong, R. J. & McAneney, K. J. Relationship between radar-derived hail kinetic energy and damage to insured buildings for severe hailstorms in Eastern Australia. *Atmos. Res.* **81**(3), 215–235 (2006).
20. Willmot, E., Bussmann, S., Homeier, N., et al. Examples of ground-based hail, rain, and wind sensor networks operating in real-time. In Fort Worth: 2017 IEEE International Geoscience and Remote Sensing Symposium (IGARSS), 2017: 5987–5989.
21. Amiranashvili, A., Chikhladze, V., Gvasalia, G., et al. Statistical Characteristics of the Daily Max of Wind Speed in Kakheti in the Days with and without Hail Processes in 2017–2019. Georgia: 2020 International Scientific Conference "Modern Problems of Ecology Proceedings". 2020
22. Scherge, M. *et al.* High-speed measurements of steel–ice friction: Experiment vs. calculation. *Lubricants* **6**(1), 26 (2018).
23. Song, Z. *et al.* Honeycomb core failure mechanism of CFRP/Nomex sandwich panel under multi-angle impact of hail ice. *Int. J. Impact Eng.* **150**, 103817 (2021).
24. Lei, Y. S., Wu, B. J. & Wu, Z. H. *Hail Generality* 25 (China Meteorological Press, 1978).

Acknowledgements

The group members are deserving of the authors' gratitude for their weekly discussions and collaborative efforts.

Author contributions

Y.D.: Resources, Supervision, Funding acquisition, Writing-review & editing. W.W.: Investigation, Data curation, Formal analysis, Methodology, Writing-original draft, Writing-review & editing. Y.X.: Investigation, Methodology, Writing-review & editing. Y.L.: Methodology. T.L.: Methodology.

Funding

The current research is supported by the National Natural Science Foundation of China (Grant Nos. 52178478), Hunan Provincial Natural Science Foundation of China (No. 2022JJ30247).

Competing interests

The authors declare no competing interests.

Additional information

Correspondence and requests for materials should be addressed to Y.D.